Bulletin of the JSME Vol.2, No.5, 2015
Mechanical Engineering Journal

ROSA/LSTF experiment on a PWR station blackout transient with accident management measures and RELAP5 analyses

Takeshi TAKEDA* and Iwao OHTSU*
* Nuclear Safety Research Center, Japan Atomic Energy Agency (JAEA)
2-4 Shirane Shirakata, Tokai-mura, Naka-gun, Ibaraki 319-1195, Japan
E-mail: takeda.takeshi@jaea.go.jp

Received 24 February 2015

Abstract
An experiment on a PWR station blackout transient with the TMLB' scenario and accident management (AM) measures was conducted using the rig of safety assessment/large scale test facility (ROSA/LSTF) at Japan Atomic Energy Agency under an assumption of non-condensable gas inflow to the primary system from accumulator (ACC) tanks. The TMLB' scenario involves prolonged complete loss of alternating current power and unavailability of turbine-driven auxiliary feedwater as well as malfunction of relief valves in primary system and steam generator (SG) secondary-side system. The AM measures considered in this study are SG secondary-side depressurization by fully opening the safety valves in both SGs with the start of core uncovery and coolant injection into the secondary-side of both SGs at low pressures. The LSTF test revealed that the primary pressure started to decrease when the SG primary-to-secondary heat removal resumed soon after the coolant injection into the SG secondary-side. The primary depressurization worsened due to the gas accumulation in the SG U-tubes after the completion of ACC coolant injection. The RELAP5 code well predicted the overall trend of the major phenomena observed in the LSTF test, and indicated remaining problems in the predictions of the SG U-tube collapsed liquid level and primary mass flow rate after the gas ingress. The SG coolant injection flow rate was found to significantly affect the peak cladding temperature and the ACC actuation time through the RELAP5 sensitivity analyses.

Key words : PWR, ROSA/LSTF, Station blackout, Accident management, SG depressurization, RELAP5 code

1. Introduction

In the earthquake and tsunami-induced station blackout (SBO) accident at the Fukushima Dai-ichi boiling water reactors on 11 March 2011, alternative water injection into the reactor as a flexible applied action was performed by using fire engines due to loss of the core cooling functions (Hirano, et al., 2012; Watanabe, et al., 2012; Kim, 2014). Yoshihara (2012) has put forward the following accident management (AM) actions at a pressurized water reactor (PWR) to ensure long-term core cooling by natural circulation (NC). Feedwater into steam generator (SG) secondary-side with steam discharge into atmosphere through the SG valves is initiated at early stages of SBO with leakage from primary coolant pump seals by using the turbine-driven auxiliary feedwater (AFW) pumps switching over from the AFW pumps to fire engines at low pressures. In addition, accumulator (ACC) system of emergency core cooling system (ECCS) should be isolated by the closure of motor-operated valves located at the outlet of ACC tanks using emergency power generators when the primary pressure decreases to a certain low pressure. Several studies on the optimization of AM measures (e.g. primary-side and/or SG secondary-side depressurization) have been done for SBO scenarios through the long-term analyses of PWRs with best-estimate computer codes (Cherubini, et al., 2008; Tusheva, et al., 2012, 2014; Prošek and Cizelj, 2013). Some experimental data on PWR SBO scenarios with AM measures have been obtained by using such integral test facilities as the PSB-VVER in Russia (Bucalossi, et al., 2012) and the PKL in Germany (Umminger, et al., 2012). The obtained data, however, would be inadequate to clarify specific thermal-hydraulic phenomena due to such atypical features as small volume and low pressure in the primary system.

In the authors' previous work (Takeda and Nakamura, 2014), post-test analysis with RELAP5/MOD3.2.1.2 code

Paper No.15-00132
J-STAGE Advance Publication date: 28 August, 2015
[DOI: 10.1299/mej.15-00132]

(RELAP5 Code Development Team, 1995) was performed for one of abnormal transient tests (Kukita, et al., 1991) on a PWR SBO transient with the TMLB' scenario (USNRC, 1975), which was conducted using the large scale test facility (LSTF) (The ROSA-V Group, 2003) under the same pressure conditions as the PWR in the rig of safety assessment-V (ROSA-V) program at Japan Atomic Energy Agency in 1995. The LSTF simulates a Westinghouse-type four-loop 3423 MW (thermal) PWR by a full-height and 1/48 volumetrically-scaled two-loop system. The TMLB' scenario involves prolonged complete loss of alternating current power, including the off-site power and the on-site emergency diesel generator power, and unavailability of turbine-driven AFW as well as malfunction of relief valves in primary system and SG secondary-side system. AM measures then are needed to maintain core cooling by coolant injection from the ACC system due to unavailability of high-pressure and low-pressure injection systems of ECCS. Core temperature excursion would take place if AM measures are initiated late during the SBO transient with the TMLB' scenario, in consequence of the related LSTF tests (Anoda, et al., 1992; Watanabe and Kukita, 1993). The AM measures considered in the authors' previous work are SG secondary-side depressurization by fully opening a safety valve (SV) in one of two SGs with the start of core uncovery and coolant injection into the secondary-side of the same SG at low pressures. Sensitivity analyses on the basis of the RELAP5 post-test analysis have showed that the AM measures are effective to core cooling by the actuation of ACC system.

In this follow-up study of the authors' previous work, a ROSA/LSTF experiment was conducted simulating a PWR SBO transient with the TMLB' scenario and AM measures in 2013. The authors consider the AM measures to depressurize SG secondary-side system by fully opening the SVs in both SGs with the start of core uncovery and to inject coolant into the secondary-side of both SGs at low pressures. The LSTF test also assumed inflow of non-condensable gas (nitrogen gas) for pressurization of ACC tanks to the primary system due to failure of the ACC system isolation after the coolant injection initiation to investigate the gas inflow effects onto the long-term SBO transient. The authors have made clear the gas inflow effects in the case of PWR small-break loss-of-coolant accident with SG secondary-side depressurization by the related LSTF tests (Takeda, et al., 2013; Takeda, 2014). The non-condensable gas enters cold legs first through ECCS nozzles and migrates to hot legs through the vessel downcomer and hot leg leak simulating lines that connect the downcomer to the hot legs, as shown in Fig. 1. The non-condensable gas in the downcomer may flow into the vessel upper-head. The non-condensable gas from the hot legs and the SG inlet plena may accumulate in the SG U-tubes. The LSTF test was analyzed by the RELAP5 code to clarify the details of major phenomena. Influences of SG coolant injection flow rate and temperature onto the long-term SBO transient were studied further by the RELAP5 sensitivity analyses. This paper describes major observations in the LSTF experiment as well as the RELAP5 post-test and sensitivity analyses to clarify thermal-hydraulic responses and to understand the AM measures effectiveness for core cooling during a PWR SBO transient with the TMLB' scenario.

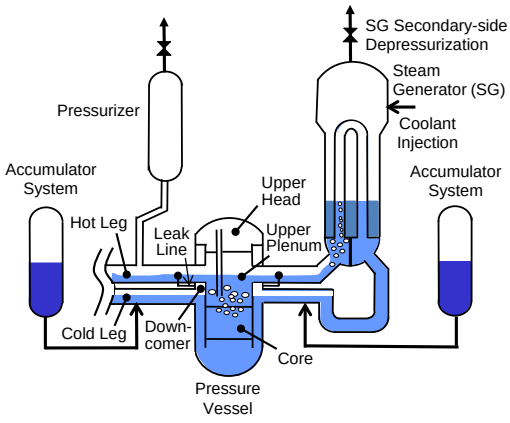

Fig. 1 Coolant behavior during PWR SBO transient with AM measures.

2. ROSA/LSTF

The ROSA/LSTF is the world largest integral test facility designed to investigate multi-dimensional thermal-hydraulic responses during PWR transients and accidents. The LSTF simulates a Westinghouse-type four-loop 3423 MWt PWR by a two-loop system model with full-height and 1/48 in volume. The reference PWR is Tsuruga Unit-2 of Japan Atomic Power Company.

Figure 2 shows the schematic view of the LSTF that is composed of a pressure vessel, pressurizer (PZR) and primary loops. Each loop includes an active SG, primary coolant pump, hot and cold legs. Loops with and without PZR are designated as loop-A and loop-B, respectively. Each SG is furnished with 141 full-size U-tubes (inner-diameter of 19.6 mm, nine different lengths as shown in Table 1), inlet and outlet plena, boiler section, steam separator, steam dome, steam dryer, main steam line, four downcomer pipes and other internals. Six U-tubes are instrumented for each SG. Instrumented U-tubes designated as tubes 1 and 6 are short tubes (type 1 in Table 1), tubes 2 and 5 are medium tubes (type 5) and tubes 3 and 4 are long tubes (type 9). The hot and cold legs, 207 mm in inner diameter, are sized to conserve the volumetric scale (2/48) and the ratio of the length to

[DOI: 10.1299/mej.15-00132]

the square root of pipe diameter to better simulate the flow regime transients in the primary loops (Zuber, 1980).

The LSTF core, 3.66 m in active height, consists of 1008 electrically heated rods in 24 rod bundles to simulate the fuel rod assembly in the reference PWR. Axial core power profile is a 9-step chopped cosine with a peaking factor of 1.495. The LSTF initial core power of 10 MW corresponds to 14% of the volumetric-scaled (1/48) PWR nominal core power because of a limitation in the capacity of power supply.

Table 1 Details of LSTF U-tubes in each SG.

Type	Straight length (m)	Number of tubes	Instrumented tubes
1	9.44	21	Two short tubes
2	9.59	19	
3	9.74	19	
4	9.89	19	
5	10.04	17	Two medium tubes
6	10.19	15	
7	10.34	13	
8	10.49	11	
9	10.64	7	Two long tubes

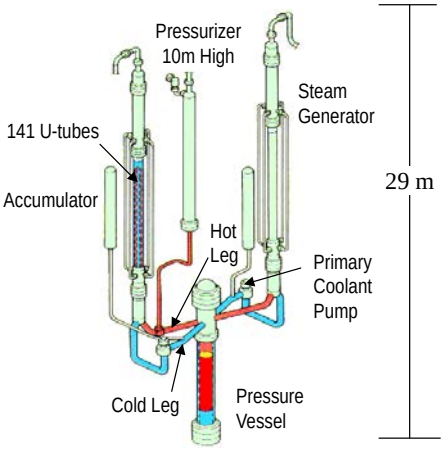

Fig. 2 Schematic view of ROSA/LSTF.

3. LSTF test and RELAP5 code analysis

3.1 LSTF test conditions

The experiment was initiated by terminating feedwater in both SGs at time zero. At the same time, a scram signal was generated, causing the closure of main steam isolation valves in both SGs. The coastdown of primary coolant pumps was started at 18 s, and the pump rotation speed was decreased to zero 250 s after the initiation of the coastdown. Initial steady-state conditions such as PZR pressure, fluid temperatures in hot and cold legs were 15.5 MPa, 597 K and 563 K, respectively, according to the reference PWR conditions. The LSTF core power decay curve after the scram signal was pre-determined based on calculations with the RELAP5 code considering delayed neutron fission power and stored heat in PWR fuel rod (Kumamaru and Tasaka, 1990) in addition to heat losses. Radial core power profile was assumed to be flat. The LSTF core power was maintained at the initial value of 10 MW for 18 s after the scram signal. The LSTF core power started to decay afterwards according to the specified core power. To obtain prototypical initial fluid temperatures with this core power, core flow rate was set to 14% of the scaled nominal flow rate. Initial SG secondary pressure was raised to 7.3 MPa to limit the primary-to-secondary heat transfer rate to 10 MW, while 6.1 MPa is nominal value in the reference PWR.

Regarding the ECCS conditions, high-pressure and low-pressure injection systems were totally failed. ACC system was automatically initiated coolant injection into both cold legs when the primary pressure decreases to 4.51 MPa according to the reference PWR. The ACC coolant injection temperature of 320 K was the same as in the reference PWR. SVs in PZR and SGs, respectively were simulated by using sharp-edge orifices of 6.83 and 16.2 mm in inner diameter, which have flow capacities corresponding to about 45% and 100% of the volumetrically-scaled flow rates of the reference PWR, due to malfunction of relief valves in PZR and SGs. Set point pressures for opening and closure of the PZR SV are 17.26 and 17.06 MPa, respectively, and those of the SG SVs are 8.68 and 7.69 MPa referring to the corresponding values in the reference PWR. Initial SG secondary-side collapsed liquid level was set to 10.3 m that corresponds to the medium tube height, similar to the authors' experiments on the PWR small-break loss-of-coolant accidents (Takeda, et al., 2013; Takeda, 2014).

As for the AM measures, SG secondary-side depressurization was done by fully opening the SVs in both SGs with the start of core uncovery. The coolant injection into the secondary-side of both SGs was initiated when the SG secondary pressure was lowered to 1.0 MPa. The coolant injection flow rate for each SG was at a constant value of 0.25 kg/s until the whole core quench is observed (to be shown in Fig. 12(a)). The SG coolant injection temperature of 415 K then was close to the saturated temperature based on the secondary pressure to avoid deformation of SG structures that may take place due to thermal shock from injection of low-temperature coolant onto high-temperature structures because of empty secondary-side of SG. The coolant injection flow rate for each SG was changed at a constant value of

[DOI: 10.1299/mej.15-00132]

0.9 kg/s thereafter to investigate influences of the coolant injection flow rate onto the long-term SBO transient. The SG coolant injection temperature then was assumed to be 335 K that is higher than the AFW injection temperature of 310 K in the reference PWR.

3.2 RELAP5 calculation conditions

The post-test analysis was conducted with the RELAP5/MOD3.2.1.2 code by incorporating a two-phase critical flow model (Asaka, et al., 1991), which may predict the discharge rate through a sharp-edge orifice to simulate the PZR SV. Figure 3 shows a noding schematic of LSTF for RELAP5 analysis. The LSTF system is modeled in one-dimensional manner including a pressure vessel, primary loops, PZR, SGs and SG secondary-side system, The SG U-tubes were modeled by nine parallel flow channels that correspond to nine different lengths of U-tubes, namely 24 nodes for short to medium tubes (straight length of 9.44-9.89 m, four cases in Table 1) and 26 nodes for medium to long tubes (straight length of 10.04-10.64 m, five cases), for better prediction of non-uniform flow distribution during NC (Susyadi and Yonomoto, 2005; Takeda, et al., 2012).

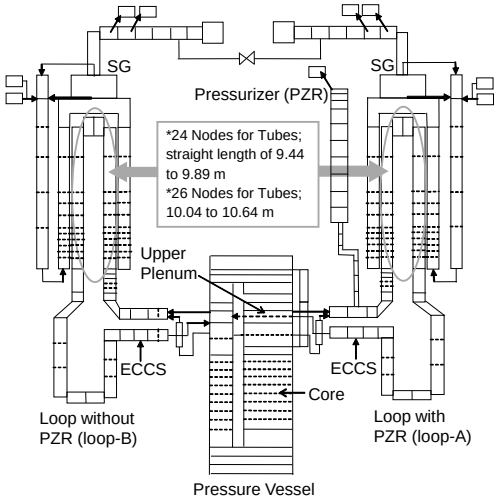

Fig. 3 Noding schematic of LSTF for RELAP5 analysis.

The core was represented by nine equal-height volumes that are vertically stacked according to 9-step chopped cosine power profile along the length of the core. The PZR was represented by ten vertical nodes to simulate corresponding facility configuration. RELAP5 liquid entrainment model for a horizontal pipe (Ardron and Bryce, 1990) was applied to the PZR surge-line inlet junction connected to the hot leg. Other initial and boundary conditions were determined according to the LSTF test data.

3.3 LSTF test and RELAP5 post-test analysis results

Table 2 summarizes the chronology of major events obtained in the LSTF test and RELAP5 post-test analysis. The LSTF test results are shown in Figs. 4-13 as a comparison with RELAP5 post-test analysis results. Table 3 summarizes the uncertainty of the LSTF test result for each of major parameters shown in Figs. 4-14, which estimated based on the instrument accuracy (The ROSA-V Group, 2003).

Table 3 Uncertainty of LSTF test result for each of major parameters.

Parameter	Uncertainty
Primary pressure	±0.108 MPa
SG secondary pressure	±0.054 MPa
SG secondary-side collapsed liquid level	±0.38 m
PZR liquid level	±0.25 m
Hot leg liquid level	±0.012 m
Collapsed liquid level in SG U-tube upflow side	±0.41 - 0.43 m
Primary mass flow rate	±1.25 kg/s
Core collapsed liquid level	±0.21 m
Cladding surface temperature	±5.31 K
ACC flow rate	±0.19 kg/s
Fluid temperature near top of SG U-tube	±2.75 K

Table 2 Chronology of major events obtained in LSTF test and RELAP5 post-test analysis.

Event	Test (s)	Cal. (s)
SG feedwater termination	0	0
SG main steam isolation valves closure	3	3
Start of primary coolant pumps coastdown	18	18
Start of single-phase liquid NC	270	270
Full PZR	7170	7250
Empty SG secondary-side	7500	7000
Termination of single-phase liquid NC	10000	9550
Start of drop in PZR liquid level	10700	9840
Empty hot leg	12130	11900
Start of core uncovery and heatup	12440	12480
Start of SG secondary-side depressurization	12460	12510
Start of coolant injection with flow rate of 0.25 kg/s for each SG	12800	12770
Appearance of PCT	13170	13070
Empty PZR	14430	14540
Start of coolant injection with flow rate of 0.9 kg/s for each SG	15360	15300
1st actuation of ACC system	16230	16540
1st termination of ACC system	17400	17830
2nd actuation of ACC system	18000	None
2nd termination of ACC system	18100	None
Start of non-condensable gas inflow to primary system	18400	17850

[DOI: 10.1299/mej.15-00132]

3.3.1 Major phenomena observed in the LSTF experiment

Figure 4 shows the primary and SG secondary pressures in loop-A. The primary pressure decreased a little because of the core power decay following the scram signal, while the SG secondary pressure rapidly increased up to about 8.6 MPa after the closure of the SG main steam isolation valves. The SG secondary pressure fluctuated between 8.68 and 7.69 MPa by cycle opening of the SG SVs until 7100 s. The SG secondary-side collapsed liquid level gradually decreased with some fluctuation because of cycle opening of the SG SVs (Figs. 4 and 5). The primary pressure turned to increase at around 4000 s when the SG secondary-side collapsed liquid level decreased to about 3 m, which caused an increase in the PZR liquid level by volumetric expansion of coolant (Figs. 4-6). The SG secondary-side liquid level became lost by 7500 s. The PZR became full of liquid at 7170 s when the PZR SV opened for the first time. Cycle opening of the PZR SV started because the primary pressure reached 17.26 MPa when the PZR liquid level was kept full, which caused loss of primary coolant. During the time period around 7170-10000 s, the primary pressure fluctuation became larger than the difference in the set point pressures for the PZR SV cycle opening probably due to influences of steam remained at the PZR top (Fig. 4).

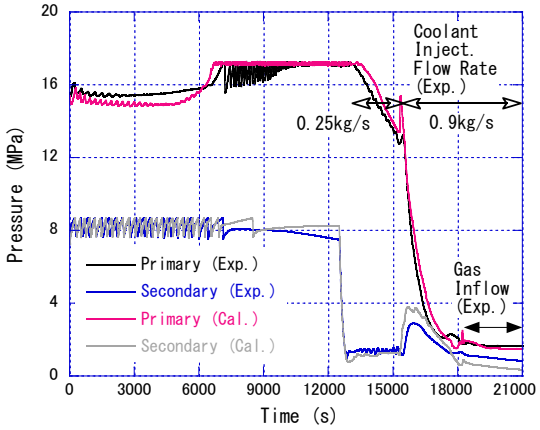

Fig. 4 LSTF and RELAP5 results for primary and SG secondary pressures in loop-A.

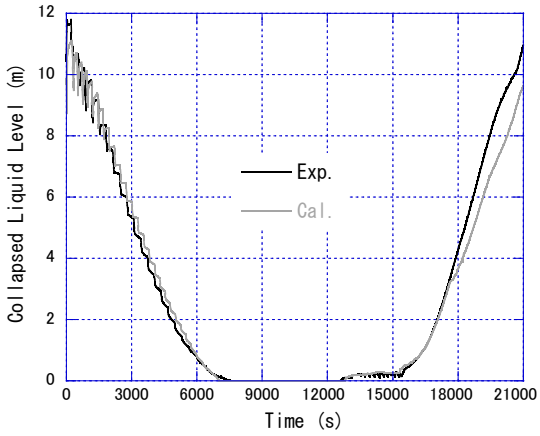

Fig. 5 LSTF and RELAP5 results for SG secondary collapsed liquid level in loop-A.

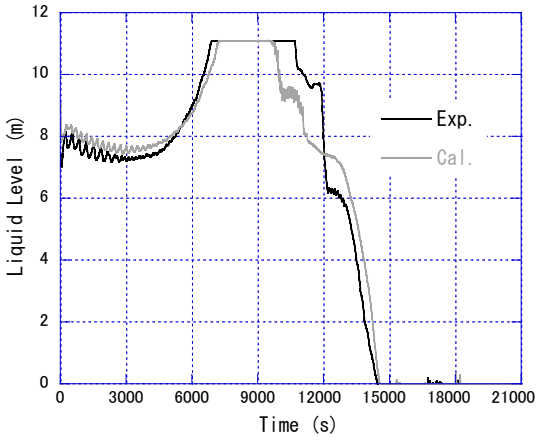

Fig. 6 LSTF and RELAP5 results for PZR liquid level.

The PZR liquid level began to drop at 10700 s after liquid level appeared in the hot leg (Figs. 6 and 7). Significant drop started in the PZR liquid level following significant decrease in the hot leg liquid level. The collapsed liquid levels in the SG U-tube upflow side in loop-A and loop-B are shown in Figs. 8 and 9, respectively. The hot leg became empty of liquid after the SG U-tubes became voided (Figs. 7-9). Figure 10 shows the primary mass flow rate in each loop. The SBO transient with the TMLB' scenario was characterized by long-term single-phase liquid NC until liquid level formed at the hot leg after the primary coolant pumps stopped (Figs. 7 and 10). The primary mass flow rate gradually decreased after the voiding started in the instrumented U-tubes at almost the same time (Figs. 8-10). Two-phase NC terminated when the primary mass flow rate decreased to zero. Liquid level in the core started to decrease following significant drop in the instrumented U-tube collapsed liquid levels (Figs. 8, 9 and 11(a)). Core uncovery and heatup took place by core boil-off at 12440 s a little after the hot leg became empty of liquid at 12130 s (Figs. 7 and 12(a)). Locations of the measuring points at Positions 5, 6, 7 and 8, respectively (shown in Figs. 11 (b) and 12 (b)) correspond to about 1.8, 2.2, 2.6 and 3.0 m above the core bottom. When the core uncovery and heatup started, the core power was 0.88 MW that corresponds to 1.2% of the volumetrically-scaled core power.

The SG secondary-side depressurization was initiated by fully opening the SG SVs at 12460 s with the start of core

[DOI: 10.1299/mej.15-00132]

uncovery, that is, the maximum cladding surface temperature reached 634 K (Fig. 12(b)). The SG secondary pressure thus decreased down to 1.0 MPa at 12800 s because of empty SG secondary-side and full steam discharge through the SG SVs. The SG primary-to-secondary heat removal resumed because of recovery of the SG secondary-side liquid level soon after the coolant injection into the SG secondary-side at the secondary pressure of 1.0 MPa, which caused decreases in the pressure and liquid level at the PZR (Figs. 4-6). The liquid levels at the core and hot leg recovered by coolant from the PZR (Figs. 7 and 11(a)). The whole core was quenched as the primary pressure decreased (Fig. 12(a)). Pressure and collapsed liquid level at the SG secondary-side were kept at around 1.3 MPa and around 0.2 m, respectively when the coolant injection flow rate for each SG was 0.25 kg/s (Fig. 4). The peak cladding temperature (PCT) was observed at Position 6 (= about 2.2 m above the core bottom). The PCT was 780 K at 13170 s. The PZR liquid level became lost by 14430 s.

After the coolant injection flow rate for each SG was changed to 0.9 kg/s at 15360 s, the SG secondary pressure once increased greatly and decreased being followed by the decreased primary pressure and the increased collapsed liquid level in the SG secondary-side (Figs. 4 and 5). As shown in Fig. 13, the ACC system started to inject coolant into both the cold legs at 16230 s, and the ACC coolant injection was temporarily terminated at 17400 s because of the primary pressure increase due to steam generation following the core liquid level increase (Fig. 11(a)). The ACC system was actuated again as the primary pressure decreased during the time period around 18000-18100 s. The liquid levels at the hot leg and SG U-tubes as well as the primary mass flow rate recovered following recovery of the primary coolant inventory after the initiation of ACC coolant injection (Figs. 7-10).

The primary depressurization was limited and pressure difference became a little larger between the primary and SG secondary sides when non-condensable gas entered the primary system after the completion of ACC coolant injection (Fig. 4). This suggests that degradation should occur in the condensation heat transfer in the SG U-tubes. The primary and SG secondary pressures were about 1.6 and 0.8 MPa, respectively, at 21000 s when the experiment was terminated. In the instrumented U-tubes (6 out of 141 in each loop), different types of flow co-existed such as those with rapid coolant drain in tube 6 (one of two short tubes) for loop-A in Fig. 8 and in tube 3 (one of two long tubes) for loop-B in Fig. 9 probably due to accumulation of non-condensable gas and those with two-phase NC with the gas causing no significant coolant drain in other instrumented tubes. Asymmetric primary mass flow rate appeared between two loops probably due to different number of forward flow SG U-tubes under influences of non-condensable gas (Fig. 10).

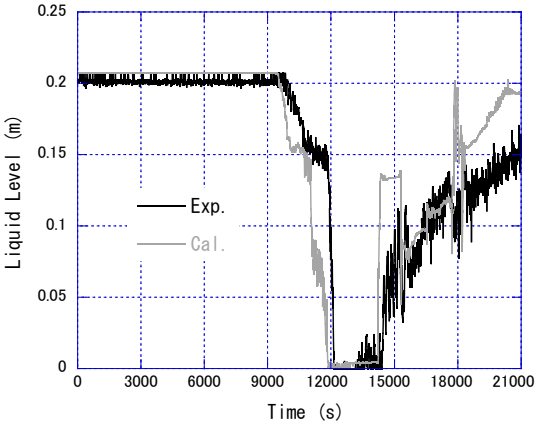

Fig. 7 LSTF and RELAP5 results for hot leg liquid level in loop-A.

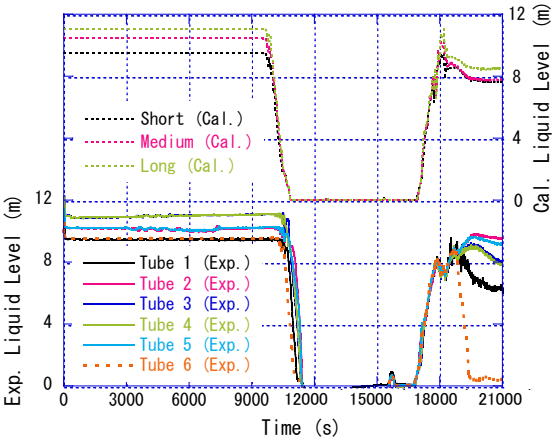

Fig. 8 LSTF and RELAP5 results for collapsed liquid levels in SG U-tube upflow side in loop-A.

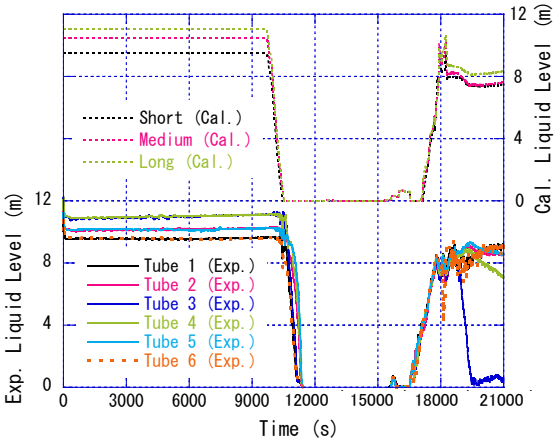

Fig. 9 LSTF and RELAP5 results for collapsed liquid levels in SG U-tube upflow side in loop-B.

[DOI: 10.1299/mej.15-00132]

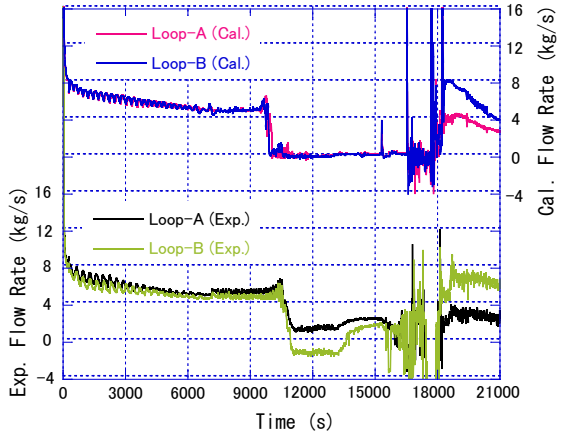

Fig. 10 LSTF and RELAP5 results for primary mass flow rate in each loop.

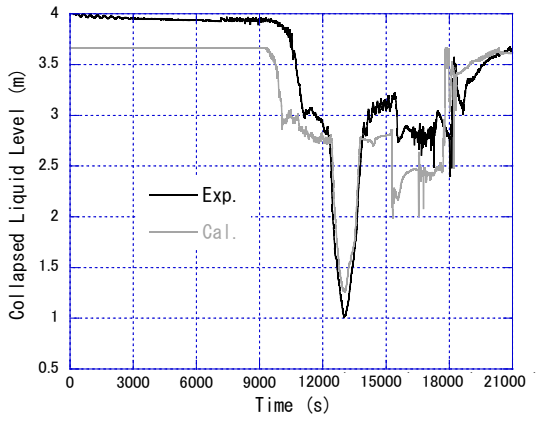

(a) Overall transient (0-21000 s)

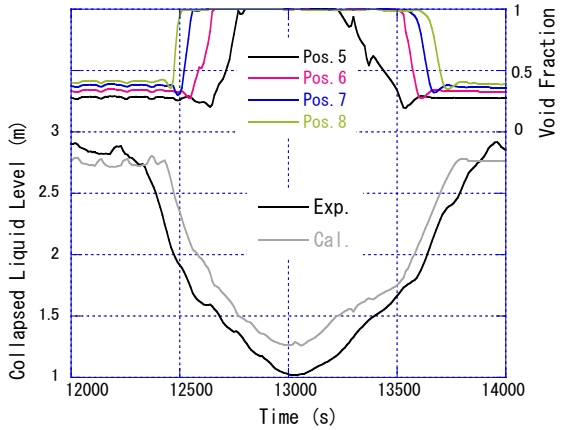

(b) Local transient (12000-14000 s)

Fig. 11 LSTF and RELAP5 results for core collapsed liquid level as well as calculated core void fraction.

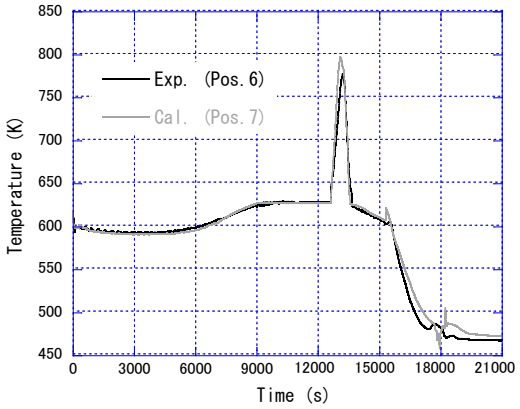

(a) Overall transient (0-21000 s)

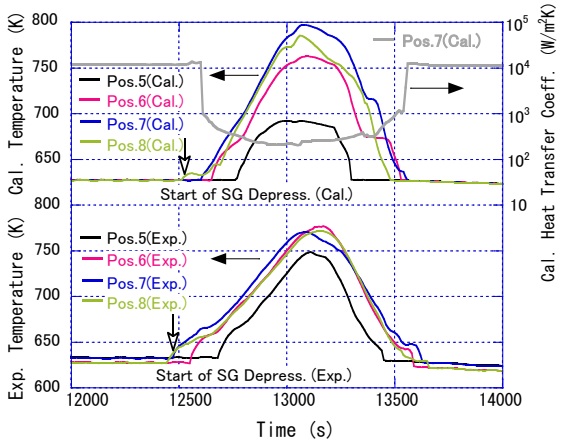

(b) Local transient (12000-14000 s)

Fig. 12 LSTF and RELAP5 results for cladding surface temperature as well as calculated surface heat transfer coefficient of cladding.

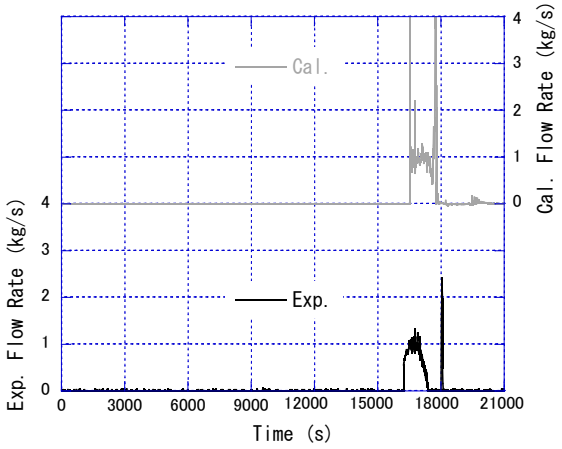

Fig. 13 LSTF and RELAP5 results for accumulator flow rate in loop-A.

[DOI: 10.1299/mej.15-00132]

Figure 14 shows the measured fluid temperatures at near the top of instrumented U-tubes shown in Table 1 in loop-A, considering the gas phase in the U-tubes after the completion of ACC coolant injection (Fig. 8). The fluid temperatures were compared with the saturated temperature based on the vessel upper plenum pressure as reference. The fluid temperatures decreased with some different rates among the U-tubes until around 19200 s, and gradually decreased in uniform manner thereafter. Trends of the fluid temperatures in the two tubes with the same length were similar to each other. The local gas phase temperatures at near the top of short, medium and long tubes became below the saturated temperature after around 18400, 18900 and 19100 s, respectively, suggesting the presence of non-condensable gas in the gas phase in the SG U-tubes (Takeda, et al., 2013).

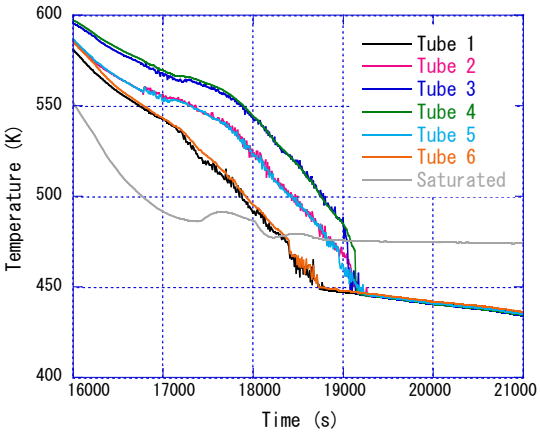

Fig. 14 Measured fluid temperatures at near top of SG U-tubes in loop-A.

3.3.2 Comparison of calculated results with LSTF data

The RELAP5 code well predicted the overall trend of thermal-hydraulic response observed in the LSTF test as compared in Figs. 4-13.

Cycle opening of the SG SVs was calculated reasonably well, which caused reasonably-well predictions of the pressure and collapsed liquid level at the SG secondary-side (Figs. 4 and 5). Some discrepancies from the measured data, however, appeared in the timings of major events as shown in Table 2. The pressure and liquid level at the PZR were underpredicted until the PZR became full of liquid (Figs. 4 and 6) because of larger number of the SG SVs cycle opening thus larger integrated discharge steam flow through the SVs due to the SVs closure at slightly lower secondary pressure obtained in the LSTF test than the set point pressure employed as the calculation condition. Significant drop started in the liquid levels at the PZR, hot leg and SG U-tubes earlier in the analysis than in the LSTF test (Figs. 6-9) because of larger number of the PZR SV cycle opening thus larger integrated discharge coolant flow through the SV. The primary mass flow rate was calculated reasonably well, though with a tendency that the flow rate decreased to zero earlier than in the LSTF test causing earlier termination of two-phase NC (Fig. 10). The hot leg thus became empty of liquid earlier in the analysis than in the LSTF test (Fig. 7).

Significant drop started in the core collapsed liquid level later in the analysis than in the LSTF test due to later initiation of the void fraction increase at the nodes near the core top, as shown in Fig. 11(b). The measuring points at Positions 5, 6, 7 and 8, respectively are located at about 1.8, 2.2, 2.6 and 3.0 m above the core bottom, while locations of the nodes of Positions 5, 6, 7 and 8, respectively correspond to about 1.6-2.0, 2.0-2.4, 2.4-2.8 and 2.8-3.2 m above the core bottom. The cladding surface temperature rises when the rod surface is uncovered above two-phase mixture level in the core. When the void fraction is 1 at a node, the core two-phase mixture level appears at just below the node. The calculated cladding surface temperatures at the nodes of Positions 5, 6, 7 and 8 began to increase at about 12740, 12650, 12610 and 12520 s, respectively when the void fraction became 1, as shown in Figs. 11(b) and 12(b). The PCT appeared at the node of Position 7 in the analysis but at Position 6 in the LSTF test because of higher minimum collapsed liquid level at the core. The PCT was overpredicted probably due to influences of the heat transfer between the cladding and coolant. The maximum cladding surface temperature at the node of Position 8 in the analysis was higher than that at Position 8 in the LSTF test, while the maximum cladding surface temperatures at the nodes of Positions 5 and 6 in the analysis were lower than those at Positions 5 and 6 in the LSTF test (Fig. 12(b)).

In the code, the single-phase steam convection regime is selected when the void fraction is above 0.999 at a node. The convective heat transfer in the single-phase steam flow is also calculated by using the maximum value among the estimation based on the correlations obtained by Dittus and Boelter for turbulent forced convection (1930), by Sellars, Tribus and Klein for laminar forced convection (1956), and by Churchill and Chu for natural convection (1975). Figure 12(b) shows the surface heat transfer coefficient of the cladding estimated from the heat flux and the temperature difference between the cladding and coolant at the node of Position 7 where the PCT appeared. The surface heat transfer coefficient of the cladding greatly decreased when the heat transfer mode became the convective heat transfer in the single-phase steam flow. The surface heat transfer coefficient of the cladding turned to increase after an increase

[DOI: 10.1299/mej.15-00132]

started in the core collapsed liquid level, which caused a decrease in the cladding surface temperature. The whole core was quenched earlier in the analysis than in the LSTF test due to higher minimum collapsed liquid level at the core.

The pressure and collapsed liquid level at the SG secondary-side as well as the primary pressure were roughly predicted when the coolant injection flow rate for each SG was 0.25 kg/s (Figs. 4 and 5). When the coolant injection flow rate for each SG was 0.9 kg/s, the primary pressure was somewhat overpredicted until the termination of ACC coolant injection, causing a little overprediction of the SG secondary pressure (Fig. 4). The ACC system was actuated once in the analysis but twice in the LSTF test due to inadequate prediction of the cold leg pressure (Fig. 13). The ACC flow rate was roughly calculated, though with a tendency that significant fluctuation appeared in the flow rate at early and last stages of the ACC coolant injection due to influences of steam condensation in the cold leg volume where fluctuation occurred in the pressure. The significant fluctuation in the ACC flow rate in the analysis caused larger fluctuation in the hot leg liquid level and the primary mass flow rate than in the LSTF test (Figs. 7 and 10).

The code reproduced degradation in the primary depressurization after the non-condensable gas inflow (Fig. 4). In the code, the condensation heat transfer under influences of non-condensable gas is calculated by using the maximum value between the estimation based on the Shah model for turbulent flow (1979) and on the Nusselt model for laminar flow (1916) with the multipliers of the Vierow-Schrock correlation (1991). The multipliers concern the heat transfer degradation expressed as a function of gas mass fraction which includes effects of the interfacial shear and the presence of non-condensable gas in a vertical tube at low pressures. A little overprediction of the pressure difference between the primary and SG secondary sides may be caused by underestimation of steam condensation in the SG U-tubes with two-phase concurrent flow.

The code reproduced a tendency of coolant drain in some of SG U-tubes after the gas inflow (Figs. 8 and 9). In the LSTF test, the collapsed liquid levels decreased with some different drain rates among the instrumented U-tubes. In the analysis, on the other hand, the collapsed liquid levels decreased with rather same drain rate among the U-tubes, even between the two SGs. The code did not properly calculate asymmetric primary mass flow rate between the two loops after the gas inflow. This was due to some discrepancies from the measured data in the SG U-tube collapsed liquid levels probably because of some differences in the gas accumulation rates between the LSTF test and the calculation (Figs. 8-10).

Calculated gas mass fractions along the length of the modeled U-tube are compared to each other to clarify the gas accumulation and distribution. Figure 15 shows the calculated gas mass fractions at the inlet, middle of upflow side, top, middle of downflow side and outlet of short, medium and long tubes in loop-A. The gas mass fractions started to increase at around 17850 s. Trends of the gas mass fractions were similar among the tubes except in early stages of the gas accumulation. The gas mass fractions at the positions other than the tube inlet greatly increased in a short time after the gas inflow, and slightly increased after around 19500 s while the SG U-tube collapsed liquid levels remained almost unchanged (Fig. 8). The calculated gas mass fraction, on the contrary, showed no

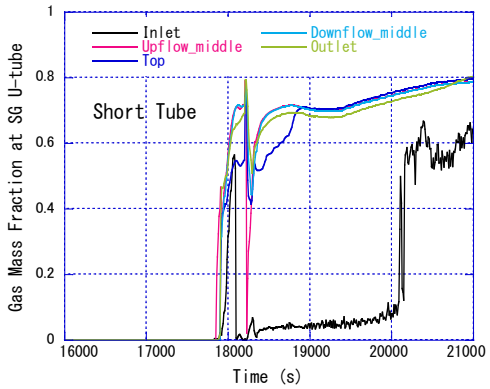

(a) Short tube

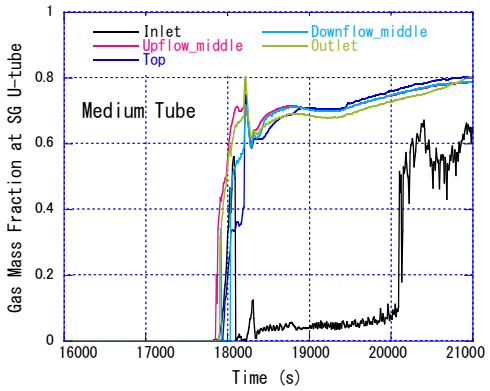

(b) Medium tube

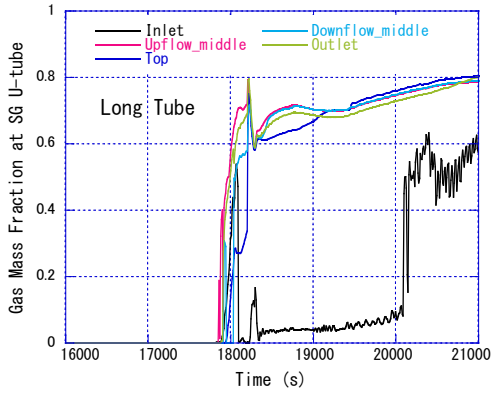

(c) Long tube

Fig. 15 Calculated gas mass fractions at SG U-tubes in loop-A by RELAP5 analysis.

[DOI: 10.1299/mej.15-00132]

accumulation of non-condensable gas in the vessel upper-head probably due to influences of steam at the upper-head by the fluid flashing because of the primary depressurization following the coolant injection into the SG secondary-side.

An insight was obtained from the RELAP5 post-test analysis that a detailed modeling of the SG U-tubes with fine-mesh multiple parallel flow channels should be needed at least when such complex thermal-hydraulic phenomena as steam condensation under non-condensable gas accumulation are involved during the SBO transient with the AM measures and the gas inflow. Calculated results by the RELAP5 code include uncertainties attributed to such individual sources as physical models (e.g. heat transfer model for condensation in the SG U-tubes under steam-gas mixture condition) and user effects (e.g. nodalization for the SG U-tubes). Analyses of the LSTF test on the SBO transient by using best-estimate plus uncertainty methods (Wilson, 2013) may be the next step.

4. RELAP5 sensitivity analyses

4.1 Sensitivity analysis conditions

Sensitivity analyses were conducted by the RELAP5 code to investigate influences of the SG coolant injection flow rate and temperature onto the long-term SBO transient. The sensitivity analysis conditions were based on the LSTF test conditions, as shown in Table 4. The SG secondary-side depressurization was initiated by fully opening the SVs in both SGs with the start of core uncovery, that is, the maximum cladding surface temperature reached 634 K. The SG coolant injection was initiated when the SG secondary pressure was lowered to 1.0 MPa. The coolant injection flow rate for each SG was at a constant value of 0.4, 0.5, 0.7 and 1.0 kg/s. The coolant injection flow rate of 0.7 kg/s for each SG corresponds to the volumetrically-scaled AFW injection flow rate of the reference PWR. The SG coolant injection temperatures of 335 and 285 K corresponded to the LSTF test condition, at which the coolant injection flow rate for each SG was 0.9 kg/s, and cold water temperature, respectively.

Table 4 Sensitivity analysis conditions.

Event or parameter	Condition
Start of SG secondary-side depressurization	Maximum cladding surface temperature of 634 K
Start of coolant injection into SG secondary-side	SG secondary pressure of 1.0 MPa
Coolant injection flow rate for each SG	0.4, 0.5, 0.7 and 1.0 kg/s
SG coolant injection temperature	335 and 285 K

4.2 Sensitivity analysis results

Figures 16-22 show the influences of the SG coolant injection flow rate onto the long-term SBO transient in the case of the SG coolant injection temperature of 335 K. The SG secondary pressure started to decrease at 12510 s when the SG SVs were fully opened. The SG coolant injection was initiated at 12770 s when the SG secondary pressure decreased down to 1.0 MPa. The PCT, which appeared at the node of Position 7, was 735, 728, 723 and 709 K at 12970, 12920, 12870 and 12830 s when the coolant injection flow rate for each SG was 0.4, 0.5, 0.7 and 1.0 kg/s, respectively (Table 5 and Fig. 22). As the SG coolant injection flow rate was larger, the PCT was lower and the whole core was quenched earlier because of faster liquid level recovery at the core and hot leg by coolant from the PZR (Figs. 19-21). The PCT was lower in the sensitivity analyses than 797 K obtained in the post-test analysis, because the coolant injection flow rate for each SG was larger than 0.25 kg/s used as the post-test analysis condition until the whole core quench.

Table 5 Sensitivity analysis results.

Coolant flow rate	PCT		ACC actuation time	
	Coolant 335 K	Coolant 285 K	Coolant 335 K	Coolant 285 K
0.4 kg/s	735 K	732 K	15370 s	15100 s
0.5 kg/s	728 K	727 K	14720 s	14540 s
0.7 kg/s	723 K	721 K	14130 s	14030 s
1.0 kg/s	709 K	709 K	13790 s	13710 s

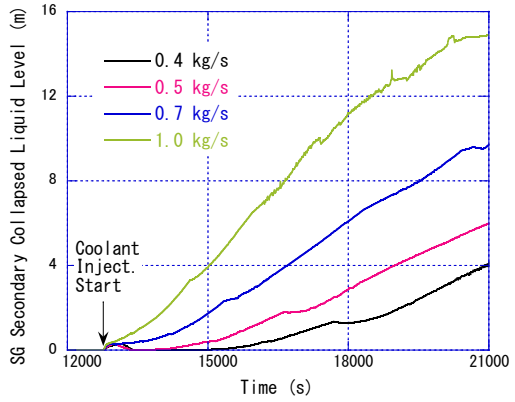

Fig. 16 Influences of SG coolant injection flow rate onto SG secondary-side collapsed liquid level in loop-A at temperature of 335 K by RELAP5 analyses.

[DOI: 10.1299/mej.15-00132]

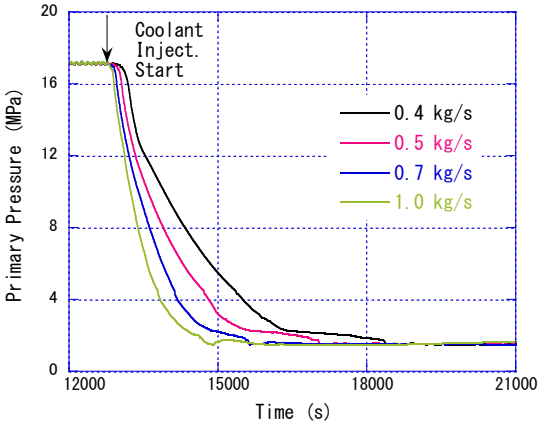

Fig. 17 Influences of SG coolant injection flow rate onto primary pressure at temperature of 335 K by RELAP5 analyses.

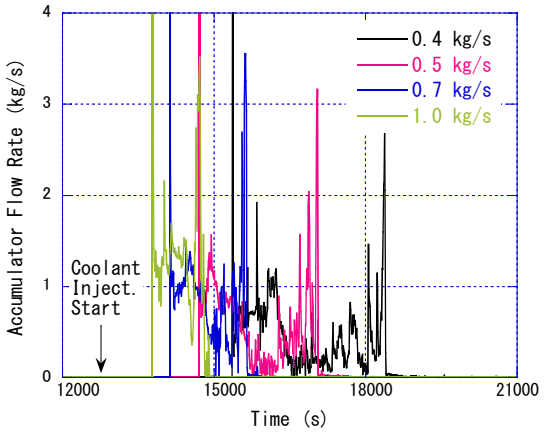

Fig. 18 Influences of SG coolant injection flow rate onto accumulator flow rate in loop-A at temperature of 335 K by RELAP5 analyses.

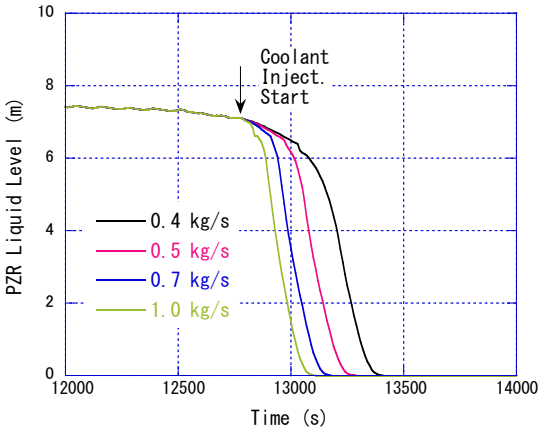

Fig. 19 Influences of SG coolant injection flow rate onto PZR liquid level at temperature of 335 K by RELAP5 analyses.

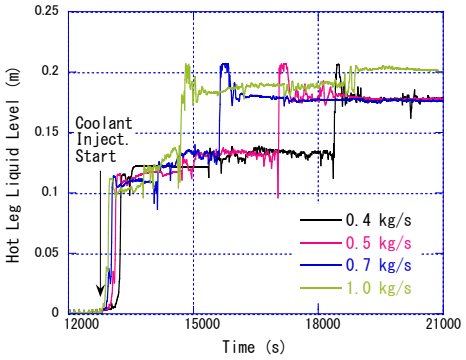

(a) Local transient (12000-21000 s)

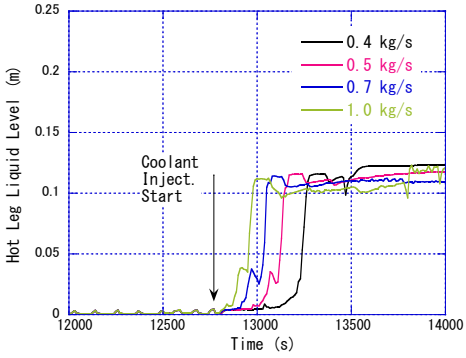

(b) Local transient (12000-14000 s)

Fig. 20 Influences of SG coolant injection flow rate onto hot leg liquid level at temperature of 335 K by RELAP5 analyses.

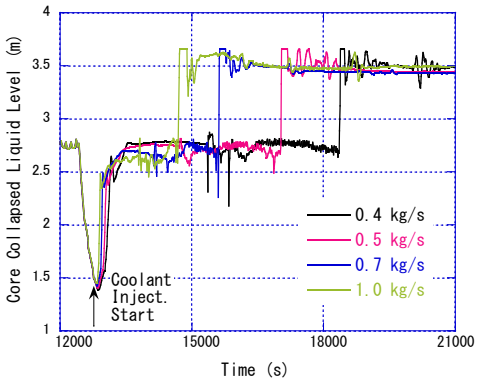

(a) Local transient (12000-21000 s)

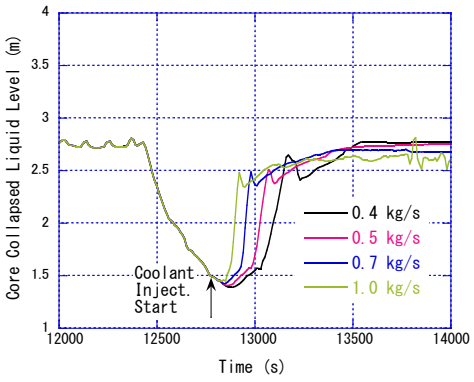

(b) Local transient (12000-14000 s)

Fig. 21 Influences of SG coolant injection flow rate onto core collapsed liquid level at temperature of 335 K by RELAP5 analyses.

[DOI: 10.1299/mej.15-00132]

The ACC system initiated coolant injection into both the cold legs when the primary pressure decreases to 4.51 MPa. The ACC coolant injection started at 15370, 14720, 14130 and 13790 s when the coolant injection flow rate for each SG was 0.4, 0.5, 0.7 and 1.0 kg/s, respectively, causing the whole core recovery by two-phase mixture (Table 5, Figs. 18 and 21). As the SG coolant injection flow rate was larger, the ACC coolant injection started earlier because of faster decrease in the primary pressure due to more effective heat removal by the SGs (Figs. 16-18).

In the case of the SG coolant injection temperature of 285 K, in contrast, the calculated results for the PCT which appeared at the node of Position 7 and the ACC actuation time are shown in Table 5. The PCT was 732, 727, 721 and 709 K at 12950, 12900, 12870 and 12830 s when the coolant injection flow rate for each SG was 0.4, 0.5, 0.7 and 1.0 kg/s, respectively. On the other hand, the ACC coolant injection started at 15100, 14540, 14030 and 13710 s, respectively.

The influences of the SG coolant injection flow rate were significant as above onto the PCT and the ACC actuation time. When the SG coolant injection flow rate and temperature were 1.0 kg/s and 285 K respectively, the PCT was the minimum and the ACC coolant injection started the earliest among the calculation cases. The SG coolant injection temperature had no significant effects onto the PCT due to no large difference of the PCT appearance time in the cases of the different injection temperatures under the same condition of SG coolant injection flow rate. On the other hand, the SG coolant injection temperature was more sensitive to the ACC actuation time because of slower decrease in the primary pressure as the SG coolant injection flow rate was smaller. Owing to influences of non-condensable gas after the completion of ACC coolant injection, however, the primary pressure remained at about 1.5-1.6 MPa at 21000 s (Fig. 23), similar to the LSTF test and RELAP5 post-test analysis.

Primary-side depressurization by fully opening the PZR SV as an optional AM action causes fast decrease in the primary pressure with fast loss of the primary coolant inventory. Influences of a combination of primary-side and SG secondary-side depressurization onto the primary pressure were investigated through a ROSA/LSTF experiment, which was carried out on AM measures during a PWR SBO transient with the TMLB' scenario and leakage from primary coolant pump seals under an assumption of non-condensable gas inflow in 2014 (Takeda and Ohtsu, 2015). The pump seal leakage was simulated by a 0.1% cold leg break. Concerning the AM measures, the SG coolant injection was initiated when the SG secondary pressure was lowered to 1.0 MPa after the combination of the depressurization with the start of core uncovery. The coolant injection flow rate for each SG and the SG coolant injection temperature were 0.7 kg/s and 310 K,

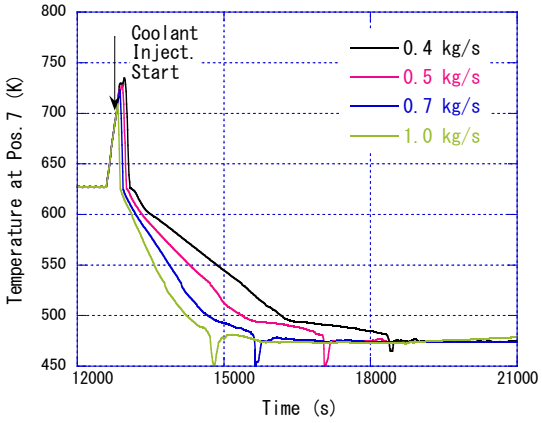

(a) Local transient (12000-21000 s)

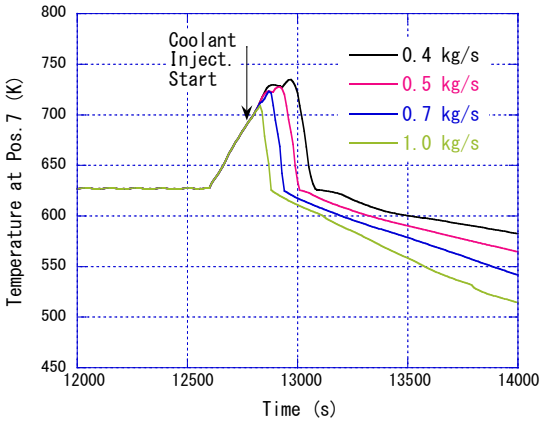

(b) Local transient (12000-14000 s)

Fig. 22 Influences of SG coolant injection flow rate onto peak cladding temperature at temperature of 335 K by RELAP5 analyses.

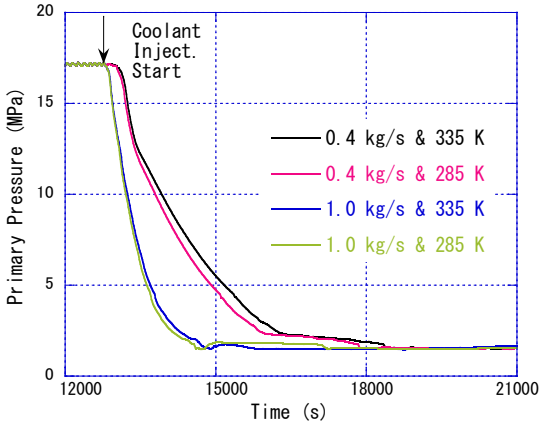

Fig. 23 Influences of SG coolant injection flow rate and temperature onto primary pressure by RELAP5 analyses.

[DOI: 10.1299/mej.15-00132]

respectively. Results of the LSTF test with the combination of the depressurization confirmed that the primary pressure remained at about 1.2 MPa due to the gas accumulation in the SG U-tubes when the test was terminated. This suggests that enhanced primary depressurization should be needed for long-term core cooling by coolant injection from systems relying on low-head pump (e.g. fire engine).

5. Conclusions

A ROSA/LSTF experiment was performed simulating a PWR SBO transient with the TMLB' scenario and AM measures. The AM measures considered in this study are SG secondary-side depressurization by fully opening the SVs in both SGs with the start of core uncovery and coolant injection into the secondary-side of both SGs at low pressures. In addition, non-condensable gas inflow to the primary system from ACC tanks was assumed due to failure of the ACC system isolation after the coolant injection initiation. RELAP5/MOD3.2.1.2 code was used for this study to clarify the details of major phenomena. Sensitivity analyses were conducted further to investigate influences of SG coolant injection flow rate and temperature onto the long-term SBO transient. Major results are summarized as follows;

1. In the LSTF test, the primary and SG secondary pressures were kept almost constant for a long time because of cycle opening of the SVs in PZR and SGs. Core uncovery and heatup took place by core boil-off a little after hot leg became empty of liquid. The SG secondary pressure rapidly decreased down to low pressure because of empty SG secondary-side and full steam discharge through the SG SVs. The primary pressure started to decrease when the SG primary-to-secondary heat removal resumed because of recovery of the SG secondary-side liquid level soon after the coolant injection into the SG secondary-side at low pressures. The liquid levels at the core and hot leg recovered by coolant from the PZR, and the whole core was quenched as the primary pressure decreased. The primary depressurization was obstructed due to the gas accumulation in the SG U-tubes after the completion of ACC coolant injection.
2. The RELAP5 code well predicted the overall trend of the major phenomena observed in the LSTF test. Significant drop in the liquid levels at the PZR, hot leg and SG U-tubes, however, started earlier in the analysis than in the LSTF test because of larger number of the PZR SV cycle opening thus larger integrated discharge coolant flow through the PZR SV. The pressure difference between the primary and SG secondary sides was a little overpredicted after the gas inflow, which may be caused by underestimation of steam condensation in the SG U-tubes with two-phase concurrent flow. The tendency of coolant drain was reproduced in some of SG U-tubes after the gas ingress. Some discrepancies from the measured data in the SG U-tube collapsed liquid levels, however, caused inadequate prediction of asymmetric primary mass flow rate between two loops.
3. The RELAP5 sensitivity analyses indicated that the PCT and the ACC actuation time were greatly dependent on the SG coolant injection flow rate. The SG coolant injection temperature was more sensitive to the ACC actuation time as the SG coolant injection flow rate was smaller, but it had no significant effects onto the PCT. Owing to influences of non-condensable gas after the completion of ACC coolant injection, however, the primary pressure remained at about 1.5-1.6 MPa at 21000 s, similar to the LSTF test and RELAP5 post-test analysis.

Nomenclature

ACC	accumulator
AFW	auxiliary feedwater
AM	accident management
ECCS	emergency core cooling system
LSTF	large scale test facility
NC	natural circulation
PCT	peak cladding temperature
PKL	Primärkreisläufe Versuchsanlage (primary coolant loop test facility)
PSB	Polnomasshtabnyi Stend Besopasnosti (full-scale safety mock-up)
PWR	pressurized water reactor
PZR	pressurizer
ROSA	rig of safety assessment

[DOI: 10.1299/mej.15-00132]

SBO station blackout
SG steam generator
SV safety valve
TMLB' T (transient event) M (failure of the secondary system relief valves and the power conversion system) L (failure of the secondary system relief valves and the auxiliary feedwater system) B' (failure to recover either on-site or off-site electric power within about 1-3 h following an initiating transient which is a loss of off-site alternating current power) (USNRC, 1975)
USNRC United States nuclear regulatory commission
VVER Vodo-Vodianoi Energeticheskii Reaktor (Russian type PWR)

Acknowledgements

Authors would like to thank to Messrs. M. Ogawa and A. Ohwada of Japan Atomic Energy Agency for performing the LSTF test under collaboration with members from Nuclear Engineering Co. as well as Miss K. Toyoda of IX Knowledge Inc. for manipulating the experimental data. Authors are grateful to Mr. K. Umminger of AREVA NP GmbH for his useful comments on the RELAP5 sensitivity analyses.

References

Anoda, Y., Katayama, J., Kukita, Y. and Mandl, R., Secondary bleed and passive feed during PWR station blackout (TMLB') transient: experimental simulation at full pressure and temperature, Proceedings of the 113th ASME Winter Annual Meeting (1992), pp. 89–96.

Ardron, K. H. and Bryce, W. M., Assessment of horizontal stratification entrainment model in RELAP5/MOD2 by comparison with separate effects experiments, Nuclear Engineering and Design, Vol. 122, No. 1-3 (1990), pp. 263–271.

Asaka, H., Kukita, Y., Yonomoto, T. and Tasaka, K., Results of 0.5% hot-leg break loss-of-coolant accident experiments at ROSA-IV/LSTF: the effect of break orientation, Nuclear Technology, Vol. 96 (1991), pp. 202–214.

Bucalossi, A., Del Nevo, A. and Morettic, F., et al., Investigation of accident management procedures related to loss of feedwater and station blackout in PSB-VVER integral test facility, Nuclear Engineering and Design, Vol. 250 (2012), pp. 633–645.

Cherubini, M., Muellner, N., D'Auria, F. and Petrangeli, G., Application of an optimized AM procedure following a SBO in a VVER-1000, Nuclear Engineering and Design, Vol. 238, No. 1 (2008), pp. 74–80.

Churchill, S. W. and Chu, H. H. S., Correlating equations for laminar and turbulent free convection from a vertical plate, International Journal of Heat and Mass Transfer, Vol. 18, No. 11 (1975), pp. 1323–1329.

Dittus, F. W. and Boelter, L. M. K., Heat transfer in automobile radiators of the tubular type, Publications in Engineering, University of California Press, Berkeley, U.S., Vol. 2, No. 13 (1930), pp. 443–461.

Hirano, M., Yonomoto, T. and Ishigaki, M., et al., Insights from review and analysis of the Fukushima Dai-ichi accident, Journal of Nuclear Science and Technology, Vol. 49, No. 1 (2012), pp. 1–17.

Kim, M.-C., Insights on accident information and system operations during Fukushima events, Science and Technology of Nuclear Installations, Article ID 123240 (2014), 12 pages.

Kukita, Y., Anoda, Y. and Tasaka, K., Summary of ROSA-IV LSTF first-phase test program –Integral simulation of PWR small-break LOCAs and transients–, Nuclear Engineering and Design, Vol. 131, No. 1 (1991), pp. 101–111.

Kumamaru, H. and Tasaka, K., Recalculation of simulated post-scram core power decay curve for use in ROSA-IV/LSTF experiments on PWR small-break LOCAs and transients, Report JAERI-M 90-142, Japan Atomic Energy Research Institute (1990).

Nusselt, W. A., The surface condensation of water vapor, Zeitschrift des Vereines Deutsch Ingenieure, Vol. 60 (1916), pp. 541–546.

Prošek, A. and Cizelj, L., Long-term station blackout accident analyses of a PWR with RELAP5/MOD3.3, Science and Technology of Nuclear Installations, Article ID 851987 (2013), 15 pages.

[DOI: 10.1299/mej.15-00132]

RELAP5 Code Development Team, RELAP5/MOD3 code manual, NUREG/CR-5535 (INEL-95/0174), Idaho National Engineering Laboratory (1995).

Sellars, J. R., Tribus, M and Klein, J. S., Heat transfer to laminar flows in a round tube or flat conduit: the Graetz problem extended, Transactions of the ASME, Vol. 78 (1956), pp. 441–448.

Shah, M. M., A general correlation for heat transfer during film condensation inside pipes, International Journal of Heat and Mass Transfer, Vol. 22, No. 4 (1979), pp. 547–556.

Susyadi and Yonomoto, T., Analysis on non uniform flow in steam generator during steady state natural circulation cooling, Report JAERI-Research 2005-011, Japan Atomic Energy Research Institute (2005).

Takeda, T., Asaka, H. and Nakamura, H., RELAP5 analysis of OECD/NEA ROSA Project experiment simulating a PWR loss-of-feedwater transient with high-power natural circulation, Science and Technology of Nuclear Installations, Article ID 957285 (2012), 15 pages.

Takeda, T., RELAP5 Analyses of ROSA/LSTF experiments on AM measures during PWR vessel bottom small-break LOCAs with gas inflow, International Journal of Nuclear Energy, Article ID 803470 (2014), 17 pages.

Takeda, T. and Nakamura, H., RELAP5 code study of ROSA/LSTF experiment on a PWR station blackout (TMLB') transient, Mechanical Engineering Journal, Vol. 1, No. 4 (2014), Paper No.13–00324, 13 pages.

Takeda, T. and Ohtsu, I., ROSA/LSTF experiment on accident management measures during a PWR station blackout transient with pump seal leakage and RELAP5 analyses, Journal of Energy and Power Sources, Vol. 2, No. 7 (2015), pp. 274–290.

Takeda, T., Ohwada, A. and Nakamura, H., Measurement of non-condensable gas in a PWR small-break LOCA simulation test with LSTF for OECD/NEA ROSA Project and RELAP5 post-test analysis, Experimental Thermal and Fluid Science, Vol. 51 (2013), pp. 112–121.

The ROSA-V Group, ROSA-V large scale test facility (LSTF) system description for the third and fourth simulated fuel assemblies, Report JAERI-Tech 2003-037, Japan Atomic Energy Research Institute (2003).

Tusheva, P., Schäfer, F. and Kliem, S., Investigations on optimization of accident management measures following a station blackout accident in a VVER-1000 pressurized water reactor, Proceedings of the International Congress on Advances in Nuclear Power Plants (ICAPP'12) (2012), Paper No.12159.

Tusheva, P., Schäfer, F. and Reinke, N., et al., Assessment of accident management measures on early in-vessel station blackout sequence at VVER-1000 pressurized water reactors, Nuclear Engineering and Design, Vol. 277 (2014), pp. 106–116.

Umminger, K., Dennhardt, L., Schollenberger, S. and Schoen, B., Integral test facility PKL: experimental PWR accident investigation, Science and Technology of Nuclear Installations, Article ID 891056 (2012), 16 pages.

USNRC, Reactor safety study – An assessment of risks in U.S. commercial nuclear power plants, Tech. Rep. WASH-1400 (NUREG-075/14) (1975).

Vierow, K. M. and Schrock, V. E., Condensation in a natural circulation loop with non-condensable gases part I – heat transfer, Proceedings of International Conference on Multiphase Flows '91 (1991), pp. 183–186.

Watanabe, T. and Kukita, Y., Experiment and analyses of PWR station blackout transient involving pump seal leak, Proceedings of the 6th International Topical Meeting on Nuclear Reactor Thermal Hydraulics (NURETH-6) (1993), pp. 1232–1239.

Watanabe, T., Ishigaki, M. and Hirano, M., Analysis of BWR long-term station blackout accident using TRAC-BF1, Annals of Nuclear Energy, Vol. 49 (2012), pp. 223–226.

Wilson, G. E., Historical insights in the development of best estimate plus uncertainty safety analysis, Annals of Nuclear Energy, Vol. 52 (2013), pp. 2–9.

Yoshihara, K., Current situation of safety assurance measures in the light of Fukushima Daiichi accident taken by Kansai Electric Power Co., Inc., Journal of the Atomic Energy Society of Japan, Vol. 54, No. 7 (2012), pp. 441–446 (in Japanese).

Zuber, N., Problems in modeling small break LOCA, NUREG-0724 (1980).

[DOI: 10.1299/mej.15-00132]